RSC Advances




ROYAL SOCIETY OF CHEMISTRY

www.rsc.org/advances

# Characterization and antifouling properties of polyethylene glycol added PAN-CAP blend membrane

Mrinmoy Mondal and Sirshendu De*

Department of Chemical Engineering

Indian Institute of Technology, Kharagpur

Kharagpur – 721302; India

* Corresponding author

Tel: + 91 – 3222 – 283926

Fax: +91 – 3222 - 255303

e-mail:sde@che.iitkgp.ernet.in

**Abstract**

Effects of polyethylene glycol (PEG) as an additive to cellulose acetate phthalate-polyacrylonitrile blend membrane in ultrafiltration range were investigated. Influence of both molecular weight and concentration of PEG were examined. Ternary phase diagrams were generated to identify the domain of composition where thermodynamic instability occurred. Kinetic hindrance due to presence of additive was also estimated. Relative importance between thermodynamic and kinetic factors was investigated quantitatively to interpret the nature of membrane morphology. Prepared membranes were characterized in terms of surface morphology by scanning electron microscopy, water permeability, pore density, molecular weight cut off, contact angle and breaking stress. Antifouling characteristics of prepared membranes were evaluated in terms of filtration of protein bovine serum albumin. Membranes with PEG 200 concentration 2 wt% and 6 wt% showed the best antifouling properties.

**Keywords:** Blend membranes; polyacrylonitrile; cellulose acetate phthalate; additive; permeability; antifouling properties.

## 1.0 Introduction

Due to low energy consumption and being environmental-friendly, membrane based technologies are becoming attractive unit operations in various applications, including water purification, pharmaceuticals, juice processing etc.[1-4] Non-solvent induced phase inversion is a well-known technique to prepare asymmetric polymeric membranes.[5-12] In this process, a thin, dense skin is formed over a porous sub-structure. The pore formation is a complicated phenomenon involving interplay of various parameters, like, polymer composition, coagulant temperature, type of solvent, nature and concentration of additives. Phase-inversion process must be carefully controlled to attain the desired morphology and performance.[13-15]

Fouling is the major problem in any membrane separation. Thus, preparation of anti-fouling membranes is an area of active research. To improve anti-fouling characteristics of the membrane surface, various methods are employed. These are blending of polymers,[10, 16, 17] addition of inorganic salts,[18, 19] surface adsorption by suitable chemical,[20,21]chemical grafting,[22, 23]UV assisted grafting,[24, 25]and plasma treatment.[26, 27] The common purpose of all these processes is to make the membrane surface more hydrophilic and fouling resistant.

Polymer blending and use of additives are one of the cost-effective methods. Sivakumar et al., reported characterization and application of cellulose acetate-polyurethane and cellulose acetate-polysulfone blend membranes.[28-31] Saljoughi et al.,[13, 32] investigated the effects of additives, like, polyvinyl pyrrolidone (PVP), polyethylene glycol (PEG) on cellulose acetate blend membrane. Rahimpour et al.,[14] used cellulose acetate phthalate (CAP) to improve the hydrophilicity of the polyethersulfone (PES) membrane. Reports are available on polysulfone–polyurethane,[33] polyvinylidene fluoride (PVDF)–polyethersulfone blend membranes.[34] These membranes were for water treatment and industrial use. Similarly, preparation of antifouling, blood and biocompatible membranes were attempted for medical applications as well. Nie et al.,[35] developed a blood and cell compatible membrane using blend of polyethersulfone, sulfonated polyethersulfone and carboxylic polyethersulfone having a heparin like surface. Ma et al.,[36] reported a new multifunctional polyethersulfone membrane coated by dopamine grafted sulfonated linear heparin-like polymer showing remarkable blood and cell compatibility. A composite layer was deposited on a polyethersulfone membrane substrate by the layer-by-layer self-assembly of graphene-based supermolecules prepared by grafting poly(styrenesulfonate) and poly(acrylamide) onto graphene oxide through free radical polymerization and this membrane was found to be highly biocompatible and bioactive. [37] Similar types of membranes with antibacterial properties were prepared by Wang et al.[38] A high-performance antifouling and antithrombotic hemocompatible blend membrane using polyethersulfone and polyurethane was also prepared by Yin et al.[39] Liu et al.[40] constructed self-cross-linked polymer nanolayers for design of versatile biointerfaces.

However, development of blend ultrafiltration membranes having antifouling properties is an area of active research for applications in industrial wastewater and surface water treatment. Literature on blending of polyacrylonitrile (PAN) with other polymers is scant. Some of these are PES-PAN, PVDF-PAN blend membranes.[41-43] Recently, Roy and De explored PAN-CAP blend membranes in dimethylacetamide and investigated their utility for extraction of steviol glycosides from stevia extract.[44] The idea was to impart more hydrophilicity to the membrane surface by blending hydrophilic CAP to hydrophobic PAN. PAN is thermally stable, chemically resistant, commercially available at lower cost and easily soluble in solvent.[45-49] Thus, it can be preferred over popular polymer polysulfone as a suitable material for blend membranes with improved desirable properties, like, hydrophilicity, without compromising the molecular weight cut off (MWCO) of the membrane. Moreover, PAN-CAP blend is compatible as discussed in this work.

Use of different molecular weight and concentration of hydrophilic polymeric additives, like, PEG and PVP for tailor-making the surface morphology and surface properties are common.[16, 50-52] In the present work, effects of molecular weight and concentration of PEG on PAN-CAP blend membrane have been investigated. The aim is to enhance the hydrophilicity of the resultant membrane further by incorporating hydrophilic PEG. The cast membranes are characterized in terms of permeability, MWCO, hydrophilicity and surface morphology. The anti-fouling characteristics of each membrane have been examined using bovine serum albumin (BSA) solution.

## 2. Experimental

### 2.1. Materials:

CAP was purchased from M/s, G.M. Chemie Pvt. Ltd, Mumbai, India. PAN (homopolymer average molecular weight of 150 kDa) was procured from M/s, Technorbital Advanced Materials Pvt. Ltd., Kanpur, India. Solvent, N, N- dimethylformamide (DMF) was purchased from M/s, Merck (India) Ltd., Mumbai, India. PEG of average molecular weight 200 Da, 400 Da, 1.5 kDa, 4 kDa, 6 kDa, 10 kDa, 20 kDa and 35 kDa was supplied by M/s, S. R. Ltd., Mumbai, India and dextran (average molecular weight: 70 kDa) was procured from M/s, Sigma Chemicals, USA. These neutral solutes were used to evaluate the MWCO of the cast membranes. PEG was also used as additives during casting of the membranes. BSA was procured from M/s, S. R. Ltd., Mumbai, India (molecular weight: 67,000 Da). Distilled water was used as the non-solvent in the coagulation bath. The membranes were cast on a non-woven polyester fabric of thickness 118 ± 22.8 μm (product number TNW006013), supplied by M/s, Hollytex Inc., New York, USA.

### 2.2 Selection of composition of PAN-CAP blend membrane

The total polymer concentration was fixed at 19 wt% in DMF. Four compositions of PAN and CAP, i.e., 19 wt% PAN, 15 wt% PAN and 4 wt% CAP, 4 wt% PAN and 15 wt% CAP and 19 wt% CAP were studied. The blend composition, 4 wt% PAN and 15 wt% CAP, was found to have the maximum hydrophilicity along with the desirable MWCO (the results are elaborated in section 3.1). In order to enhance the hydrophilicity of the blend membrane further without compromising the MWCO, effects of molecular weight and concentration of PEG additive on this blend composition was undertaken in this study. The molecular weight of PEG was varied as 200, 400, 1500, 4000 and 6000 Da at 1 wt%. Concentration of PEG of molecular weight 200 Da was varied as 1, 2, 4, 6, 8 and 10 wt% to observe the effect of concentration.

### 2.3. Membrane Preparation

Flat sheet blend membranes were prepared by phase inversion method and hand casting. For PAN-CAP-PEG membrane, fixed amount of PEG of different molecular weight and concentration was added in premixed 15 wt% CAP and 4 wt% PAN in DMF solution and dissolved at $60^0$C. The solution was prepared under constant mechanical stirring for 6 hour at $60^0$C to mix completely and it was then cast on the non-woven polyester fabric (attached to a glass plate), with the help of a stainless steel casting knife, set at a fixed gap of 150 µm and a manual drawdown speed of 30 mm/s. The casting solution with glass plate was immediately put into a gelation bath (to minimize the evaporative effect) containing distilled water for phase inversion at room temperature. The membrane was kept in the bath for 24 hours to complete the phase inversion. The above procedure was followed for casting PAN-CAP membranes with compositions presented in earlier section.

### 2.4 Ternary phase diagram

The ternary phase diagram was constructed from the cloud point data determined by the usual titration method.[53] Phase diagrams were generated to observe the effect of PEG molecular weight (at a fixed concentration) and concentration (at a fixed molecular weight). For the former case, three compositions of casting solution were considered, i.e., no PEG, PEG 1500 Da and 6000 Da at 1 wt%. To observe the effect of PEG concentration, two concentrations of PEG-200, i.e., 6 and 10 wt% were selected. The polymer solution was stirred for 6 h. Distilled water was added dropwise into the polymer solution under stirring by using a 100 µL micro-pipette to perform the titration. At the first sign of turbidity, the addition of distilled water was stopped and the cloudy solution was stirred for an additional 30 min to see whether the turbid solution became clear. If the suspension remained turbid, the composition was recorded as the cloud point. The composition at the cloud point was determined from the amount of water, DMF and polymer present in the solution.

#### 2.4.1 Thermodynamic and kinetic instabilities of casting solution

Miscibility gap (MG) and degree of shift in binodal curve (DSBC) determine the thermodynamic properties of the casting solution.[53] Thermodynamic instability of polymeric solution with additive is represented by an enhancement parameter, T. Large value of T indicates thermodynamic instability. The detailed calculation involved for estimation of T for various compositions of casting solution is presented in Appendix A.

In addition to thermodynamic instability, solvent-nonsolvent kinetics during phase inversion is an important controlling factor for final pore size distribution in the membrane. This is quantified by kinetic hindrance parameter, K. Reduction of K indicates a denser membrane matrix. K can be quantified by measuring the concentration of solvent (DMF) in the gelation bath as a function of time. The detailed calculations involved in estimation of K are presented in Appendix A.

### 2.5. Characterization of the membranes

#### 2.5.1. Membrane permeability

Prepared membranes were compacted in an unstirred batch cell at 690 kPa for 3 hours. The batch cell (effective filtration area 33 $cm^2$) was filled by 500 ml distilled water and then steady state permeate flux was measured at five different trans-membrane pressure drop. The permeate flux was calculated by

$$J_w = Q / A_0 \Delta T_0 \quad (1)$$

where, $J_w$ is pure water flux; $Q$ is volume of permeate collected in $\Delta T_0$; $A_0$ is effective membrane surface area. A plot of $J_w$ against transmembrane pressure drop resulted in a straight line passing through the origin, the slope of which gave the membrane permeability.

#### 2.5.2 Molecular weight cut off (MWCO) of the membrane

MWCO of the membranes was calculated by measuring the rejection of neutral solutes of different molecular weights (4, 6, 10, 20, 35, 70, 100 and 200 kDa). A solution of 10 $kg/m^3$ was prepared in distilled water and fed to the batch cell under stirring. The experiments were conducted at 70 kPa transmembrane pressure drop at 2000 rpm. The permeate was analyzed and the percentage rejection (%R) was measured as:

$$R = (1 - C_P/C_F) \times 100\ \% \quad (2)$$

$C_P$ is concentration of permeate, $C_F$ is concentration of feed. Rejection values were plotted against the molecular weight of solutes in a semi-logarithmic curve. Molecular weight corresponding to 90 % rejection was estimated as MWCO.

#### 2.5.3 Contact angle:

Contact angle of the membrane was measured by a Goniometer, supplied by M/s, Rame Hart, New Jersey, USA using the sessile drop method.[54] Contact angle at six different locations were measured and average value was reported.

### 2.5.4 Pore density

Pore density was calculated using the classical Hagen-Poisseulle's equation. It was assumed that membrane had straight cylindrical pores. Thus, the volumetric flow rate is given by

$$Q = \frac{\Delta P \pi r_{avg}^4}{8 \mu L} \quad (3)$$

$r_{avg}$ was calculated using the following equation[55]:

$$r_{avg}(cm) = 16.73 \times 10^{-10} (MWCO)^{0.557} \quad (4)$$

where, $\Delta P$ is transmembrane pressure drop; $r_{avg}$ is average pore radius; μ is water viscosity; $L$ is thickness of the membrane (i.e., total thickness – thickness of the fabric). If $n_c$ = number of pores / membrane surface area, the total flux ($J_w$) is

$$J_w = Q \text{ x } n_c \quad (5)$$

Using Eqs. (3) and (5), the following expression of pore density is obtained.

$$n_c = \frac{8 J_w \mu L}{\Delta P (\pi r_{avg}^4)} \quad (6)$$

### 2.5.5 Pore volume distribution and average pore radius by BET analysis

Pore volume distribution of the prepared membrane samples was measured by Brunauer–Emmett–Teller (BET) analysis. The BET instrument was supplied by Quantachrome instruments, Florida, USA (model: AUTOSORB-1).

### 2.5.6 Surface morphology:

The surface morphology of the membranes was studied with scanning electron microscope (SEM) (model: ESM-5800, JEOL, Japan).

### 2.5.7 Atomic force microscopy (AFM)

The atomic force microscope (model: 5500 AFM, Agilent Technologies, USA) was used to measure the surface roughness of the membranes under tapping mode.

### 2.5.8 Mechanical strength:

The mechanical strength of the membranes, in terms of breaking stress was studied by a universal electronic strength measuring instrument, procured from M/s, Tinius Olsen Ltd.,

Redhill, England of model H50KS. All measurements were carried out at room temperature and strain rate of 20 mm/min. Average of three values of each sample was reported.

**2.5.9 Differential scanning calorimetry:**

The thermal analysis of pure and blend membranes were carried out in a differential scanning calorimeter (M/s, TA instrument Ltd., New castle, Delaware USA; model DSC $Q_{20}$). The experiment was carried out in a two step heating-cooling cycle in nitrogen atmosphere. The analysis was carried out utilizing 5 mg of membrane samples in an aluminium pan and heated from 0 to 300 $^0$C at a heating rate of 10$^0$C/min.

**2.5.10 Antifouling experiment using BSA:**

BSA solution of 500 mg/l at pH 7.0 and transmembrane pressure drop of 138 kPa was used to conduct antifouling experiments.

**2.5.11 Flux recovery ratio (FRR) and flux decline ratio (FDR) of membrane**

Membrane gets fouled due to the deposition of solutes after each experiment. Antifouling characteristics of the membrane were quantified with the help of two parameters i.e., flux decline ratio (FDR) and flux recovery ratio (FRR). FRR is related to the irreversible membrane fouling and was calculated by measuring the pure water flux of all the membranes before and after BSA experiments. FDR quantifies the flux decline during a particular experiment with protein solution. FRR is defined as

$$FRR = \left(\frac{J_{w2}}{J_{w1}}\right) \times 100\% \qquad (7)$$

where, $J_{w2}$ is water flux of the membrane after experiment; $J_{w1}$ is water flux of the membrane before experiment. FDR is defined as

$$FDR = \left(\frac{J_1 - J_s}{J_1}\right) \times 100\% \qquad (8)$$

where, $J_1$ is initial flux of the membrane with BSA and $J_s$ is the flux at the end of one hour.

**2.6 Analysis**

The rejection of neutral solutes for MWCO analysis was measured by a digital refractometer (supplied by M/s, Cole-Parmer, Kolkata, India). The concentration of the BSA before and after the experiments was measured with a UV-visible spectrophotometer

(supplied by M/s, Perkin Elmer, Connecticut, USA, model: Lambda 35) at wavelength 280 nm.

## 3.0 Results and discussions

### 3.1 Selection of composition of PAN-CAP blend membrane

Variation of contact angle and MWCO of PAN-CAP is presented in Table 1. It is observed that hydrophilicity of the membrane decreases as the CAP concentration increases in the blend, thereby reducing the contact angle. For example, PAN 19 wt% has contact angle $86^0$ and it decreases to $72^0$ for 15 wt% CAP blended in PAN. MWCO of the membrane increases with CAP concentration. For example, MWCO increases from 12 kDa to 85 kDa with increase in CAP concentration from 0 to 19 wt%. CAP 19 wt% membrane shows the highest hydrophilicity (contact angle $65^0$) but the MWCO (85 kDa) is higher than PAN (4 wt%)-CAP (15 wt%) blend membrane (38 kDa). This particular PAN-CAP blend results in the highest hydrophilicity and desired MWCO among the blends. Therefore, the membrane of this composition is selected to study the effects of PEG additives in order to enhance the hydrophilicity further.

**Table 1:** Contact angle and MWCO of the membrane for various composition of PAN and CAP

| Synthesized membrane | Contact Angle ($^0$) | MWCO (Da) |
|---|---|---|
| **PAN 19 wt%** | 86±2 | 12000±1100 |
| **PAN 15 wt%, CAP 4 wt%** | 78±3 | 21000±800 |
| **PAN 4 wt%, CAP 15 wt%** | 72±2 | 38000±700 |
| **CAP 19 wt%** | 65±3 | 85000±900 |

### 3.2 Ternary phase diagram, thermodynamics instability and kinetics hindrance

The phase diagram of water/PAN-CAP/DMF/PEG is shown in Fig. 1. By introducing PEG into the casting solution, the curve moves closer to the polymer/ solvent axis (Fig 1a). Therefore, less water is needed for the precipitation of polymer compared to water/DMF/PAN-CAP. This indicates that the additive lowers the thermodynamic stability of the casting solution. Addition of higher molecular weight of PEG (6 kDa) shifts the binodal curve further left, indicating lesser thermodynamic stability and lower water requirement for precipitation of polymer. Similarly, effects of concentration of PEG are clear from Fig. 1(b). Thermodynamic instability of solution increases with concentration of PEG-200.

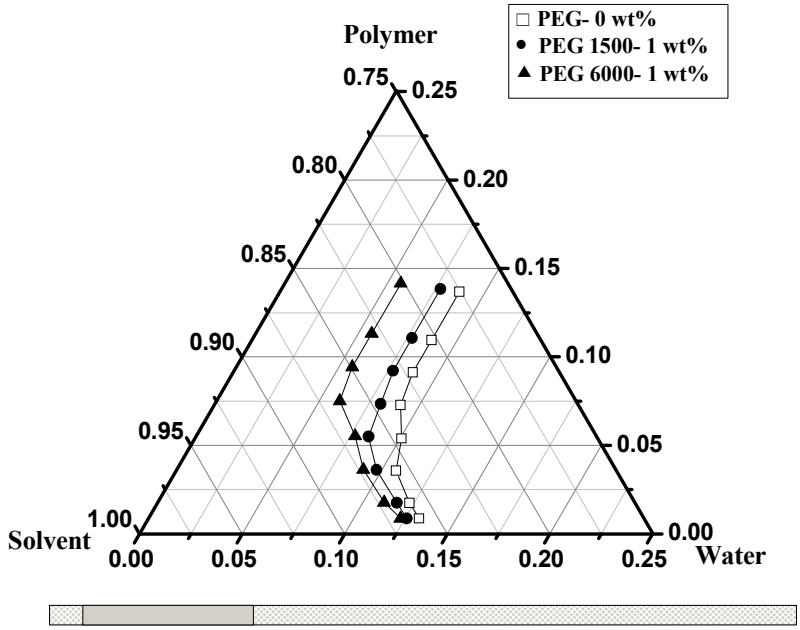


(a)

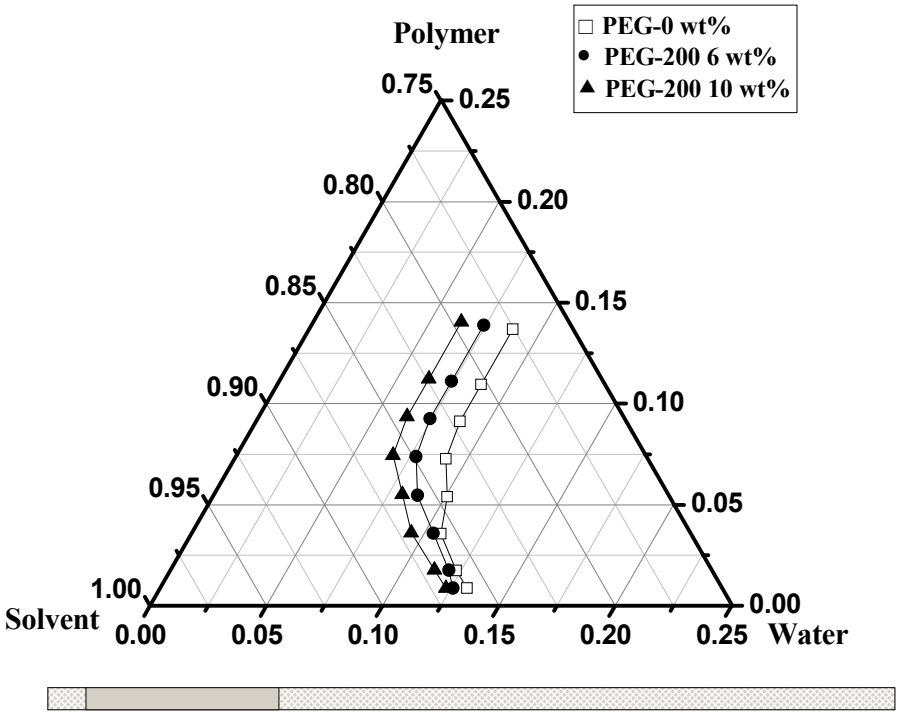


(b)

**Fig. 1:** Ternary phase diagram of Water/PAN-CAP-PEG/DMF system variation of (a) PEG Molecular weight, (b) concentration of PEG-200.

Thermodynamic stability of the casting solution is more quantitavely interpreted from thermodynamic enhancement parameter, T as elaborated in the Appendix. Values of T for various composition of casting solution are presented in Table 2. At a fixed concentration (1 wt%), T increases with molecular weight of PEG. Its value is 13 for PEG 1500 and 56.3 for PEG 6000, indicating enhanced thermodynamic instability of the casting solution resulting in the possibility of formation of porous membrane. Effects of concentration of PEG are also apparent from the T values in Table 2.

**Table 2:** Thermodynamic properties of casting solution

| Membrane | MG | DSBC (%) | $\delta_{DMF/additive}$ | $\chi_{DMF/additive}$ | T |
|---|---|---|---|---|---|
| PEG-200 0 wt% | 2.7 | 0 | - | - | - |
| PEG-200 6 wt% | 2.4 | 11.0 | 3.55 | 0.39 | 4.4 |
| PEG-200 10 wt% | 2.1 | 22.0 | 3.55 | 0.39 | 8.7 |
| PEG-1500 1 wt% | 2.4 | 11.0 | 6.11 | 1.16 | 13. 0 |
| PEG-6000 1 wt% | 1.7 | 37.0 | 6.99 | 1.52 | 56.3 |

T increases from 0 (for 0 wt% PEG-200) to 8.7 (for 10 wt% PEG-200). However, the membrane morphology is not only dependent on thermodynamic consideration but also on the kinetics of solvent-nonsolvent demixing. Kinetics of solvent-nonsolvent demixing is quantified by kinetic parameter K as explained in Appendix A.

Values of K for various compositions of casting solutions are presented in Table 3. Enhancement of 'K' indicates quick demixing leading to porous membrane and lower value of K results to delayed demixing and hence a denser membrane. As observed from Table 3, K increases from 5.9 to 8.0 with addition of 6 wt% PEG-200 in the casting solution. Actually relative magnitude of T and K for different casting solutions dictates the interplay of thermodynamic and kinetic effects. Addition of 6 wt% PEG-200 to the casting solution results in increase in both T and K indicating both effects in tandem, leading to a porous membrane. On the other hand, in case of 10 wt% PEG-200, kinetic parameter K decreases to $6.2\times10^{-9}$ and thermodynamic parameter T increases to 8.7 compared to 6 wt% PEG-200 (4.4). As discussed by Sadrzazdeh and Bhattacharjee,[53] alteration in kinetic parameter has more prominent effect than thermodynamic instability. Therefore, for 10 wt% PEG-200, kinetic hindrance is more dominant than thermodynamic instability and membrane with 10 wt% PEG-200 is expected to have a denser morphology. In case of higher molecular weight of PEG (1500 and 6000 Da), thermodynamic parameter T increases significantly (13 and 56.3

compared to 0 for no PEG) compared to marginal increases of kinetic parameter ($7.9\times10^{-9}$ and $9.6\times10^{-9}$ from $5.9\times10^{-9}$). Also, both effects are synergistic in nature. Thus, for higher molecular weight of PEG, the membrane structure is expected to be more porous.

**Table 3:** Kinetics property of casting solution

| Synthesized membrane | m ($min^{1/2}$) | $t_0$ (min) | Viscosity (μ) (Pa.s) | $Dm/\sqrt{D_s}\times10^{-3}$ (cm $min^{1/2}$) | Correlation coefficient | $K\times10^{-9}$ |
|---|---|---|---|---|---|---|
| PEG-200 0 wt% | 0.046 | 0.19 | 19.5 | 1.39 | 0.998 | 5.9 |
| PEG-200 6 wt% | 0.055 | 0.28 | 28.3 | 1.67 | 0.972 | 8.0 |
| PEG-200 10 wt% | 0.050 | 0.34 | 30.9 | 1.55 | 0.989 | 6.2 |
| PEG-1500 1 wt% | 0.060 | 0.42 | 31.1 | 1.85 | 0.990 | 7.9 |
| PEG-6000 1 wt% | 0.063 | 0.51 | 32.5 | 1.93 | 0.983 | 9.6 |

### 3.3 SEM

Effects of molecular weight of PEG (at 1 wt%) on blend membrane were studied using 200, 400, 1500, 4000 and 6000 Da of PEG. SEM images of cross section of the resultant membranes are presented in Fig. 2(a). As observed from Fig. 2(a), there is a thin and dense skin followed by a porous substructure. This is a common feature of the phase inversion membranes. General observation from this figure is that tear drop like pores start appearing under the skin layer with increase in molecular weight of PEG in the blend. The size and length of the pores increase with PEG molecular weight. The skin layer is clearly visible in Figs. 2(a) (i), (ii) and (iii). From Figs. 2(a) (i) and (iii), skin layer thickness can be estimated as less than 3 μm. The width of macropores is 20 to 40 μm for PEG 200 Da; it is 20 to 40 μm for PEG 400 Da; 20 to 45 μm for PEG 1500 Da; 30 to 50 μm for PEG 4000 and 6000 Da. The length of the macropores increases with the molecular weight of PEG. For PEG 6000 Da, the macropores cover almost the full cross section of the membranes. PEG is a well known pore former.[52] Being hydrophilic, it leaches out during phase inversion to anti-solvent (water) leaving behind macropores. With increase in molecular weight of PEG, larger sized PEG molecules create bigger pore and consequently the membrane becomes more porous. These observations are in corroboration with the thermodynamic and kinetic parameters discussed in section 3.2 that porous membrane are formed as molecular weight of PEG increases in the blend.

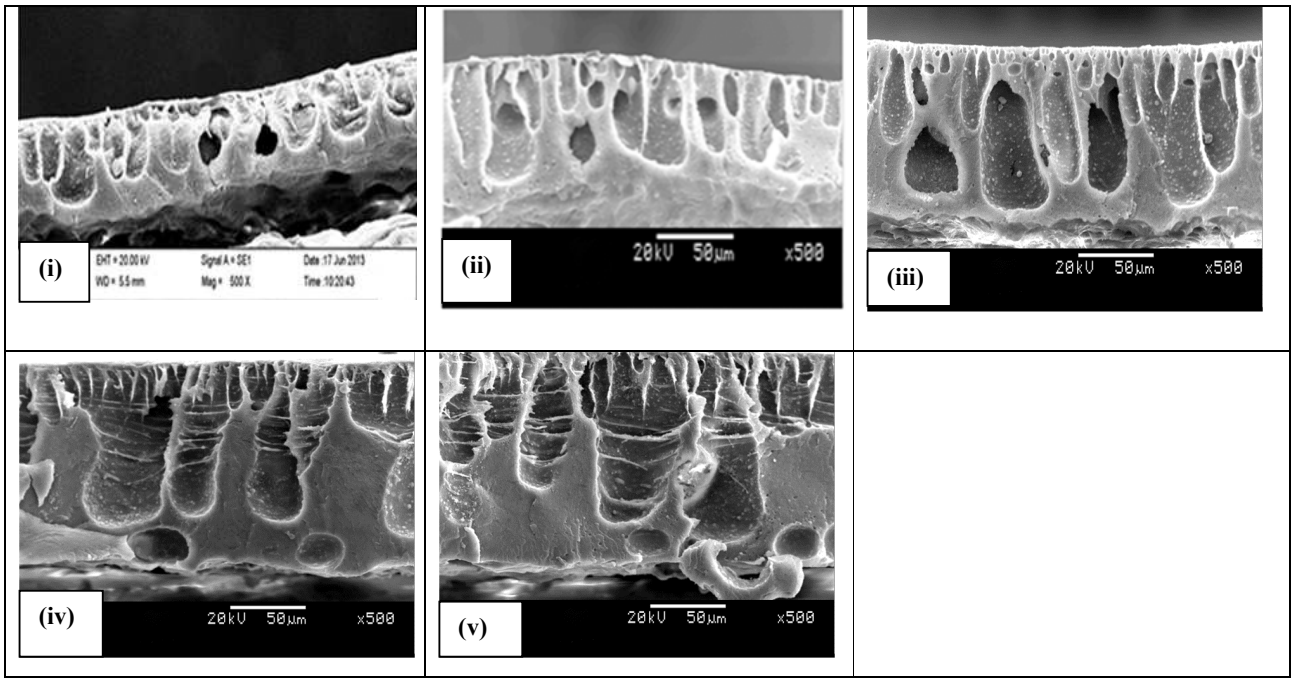


**Fig. 2(a)**: Cross section of membrane with various molecular weight of PEG (1 wt%) dope in blend (i) 200 Da, (ii) 400 Da, (iii) 1500 Da, (iv) 4000 Da, (v) 6000 Da.

Since, PEG 200 resulted less porous structure or denser membrane,[56] it was selected to study the effects of additive concentration. Concentration of PEG 200 was varied from 1 to 10 wt%. SEM images of cross section are presented in Fig. 2(b). As observed from Fig. 2(b), pore size increases with PEG concentration upto 6 wt% and the morphology becomes denser thereafter till 10 wt% (as discussed earlier). For PAN-CAP blend membrane without PEG, the size of macropores is less than 25 µm (Fig. 2(b) i). For 1 wt% PEG-200, tear drop like macropores are visible in the cross section with a pore width in the range of 10 to 40 µm. The size of pores increases when 2 wt% PEG-200 is added and pore width is in the range of 25 to 40 µm. By increasing PEG concentration to 4 and 6 wt%, wider (10 to 50 µm) and longer macropores are formed. For 8 and 10 wt% of PEG, morphology of membrane matrix changes from porous to denser structure (as discussed earlier).

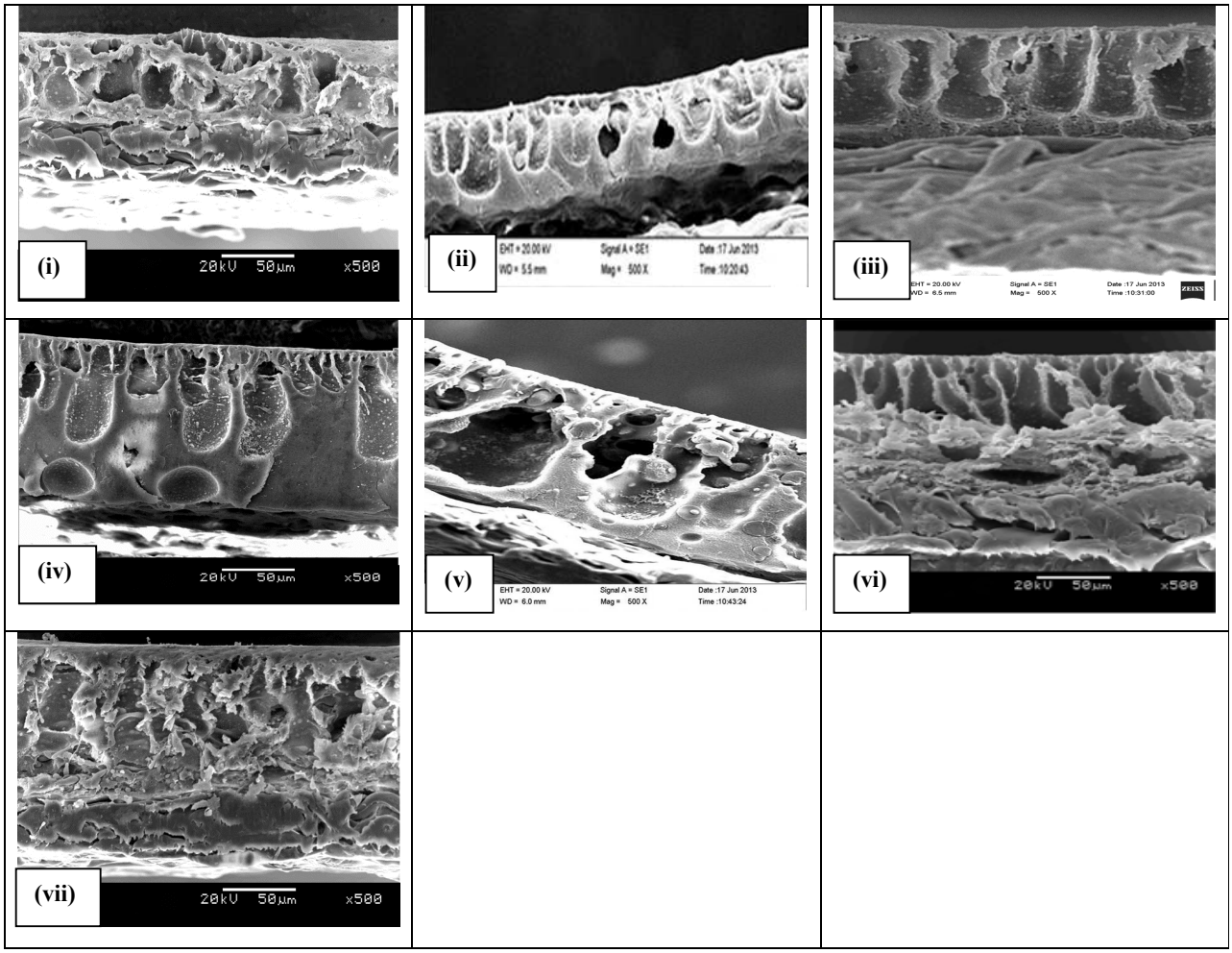


**Fig. 2(b)**: Cross section of membrane with various weight % of PEG-200 dope in blend (i) 0, (ii) 1, (iii) 2, (iv) 4, (v) 6, (vi) 8, (vii) 10.

It is observed from Fig. 2(b) (vii) that no regular contour of macropores is visible and a dense structure is formed. This phenomenon can be explained on the basis of dominance of phase inversion kinetics as discussed earlier. The size and number of pores formed during phase inversion is determined by the inter diffusion of water (non-solvent) and solvent from the membrane matrix into the gelation bath. It is a proven fact that PEG imparts hydrophilicity to a membrane matrix, and in the gelation bath, the hydrophilicity induces water to move freely into the matrix and the solvent out of it leading to bigger sized pores. This observation is in corroboration with variation of thermodynamic and kinetic parameters with composition of casting solution as discussed in earlier section. Beyond, 8 wt% PEG, kinetic hindrance parameter becomes dominant, setting in the delayed demixing, thereby, forming a denser membrane matrix.

### 3.4 Permeability and Pore density

Variation of membrane permeability and pore density as a function of molecular weight of PEG is shown in Fig. 3(a).

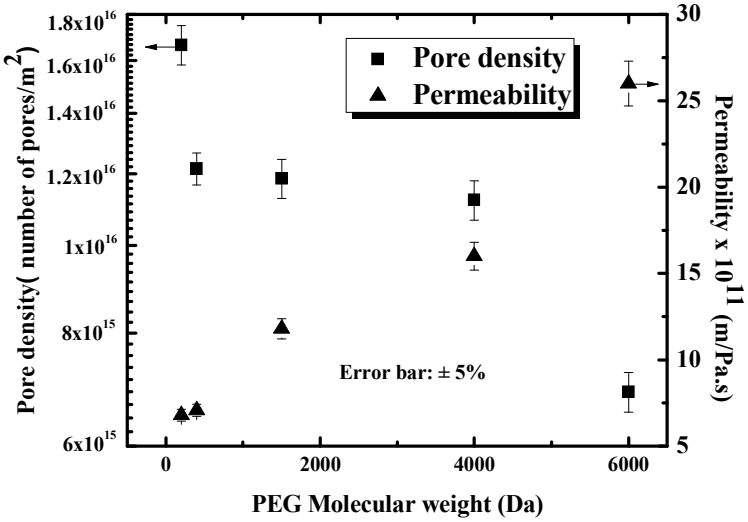


**Fig 3(a):** Pore density and permeability with variation of PEG Molecular weight

As observed from SEM images in Fig. 2(a), the membrane becomes more porous with PEG molecular weight, leading to increase in the membrane permeability. Permeability of the membrane increases from 6 x$10^{-11}$ m/Pa.s to 26 x$10^{-11}$ m/Pa.s as the molecular weight of PEG increases from 200 to 6000 Da. However, a reverse trend is observed in case of pore density. Pore density decreases from 2 x$10^{16}$ to 7 x$10^{15}$ /$m^2$ as molecular weight of PEG increases from 200 to 6000. As observed from SEM images, for cross-section in Fig. 2(a), the pore size increases but number of pores decreases with PEG molecular weight, thereby leading to decrease in pore density. Therefore, although pore density decreases, membrane permeability increases. Formation of bigger and longer macropores as discussed earlier is responsible for this behaviour.

Fig. 3(b) demonstrates the variation of membrane permeability and pore density with concentration of PEG-200.

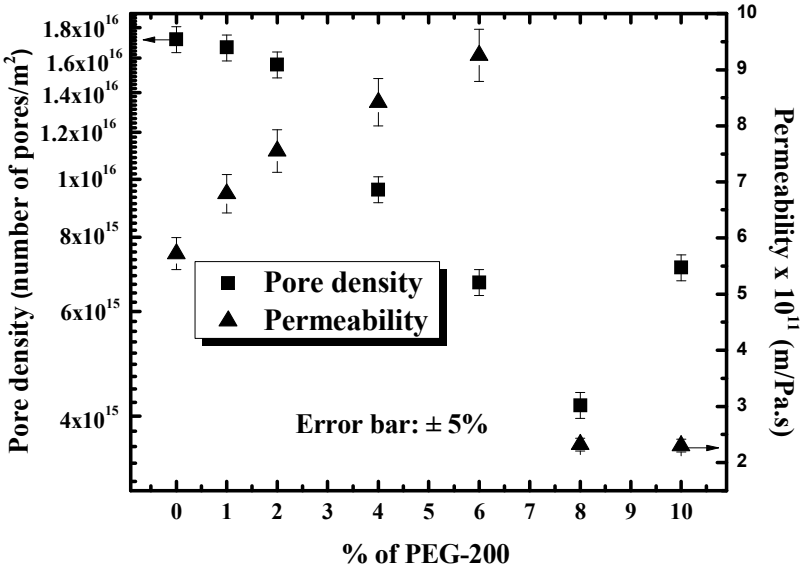


**Fig 3(b)**: Pore density and permeability with variation of concentration of PEG-200.

As observed in SEM figures (Fig. 2b), the membrane pore size increases upto 6 wt% and decreases thereafter. The same trend is reflected in membrane permeability. Permeability increases from 5.5 $x10^{-11}$ to 9 $x10^{-11}$ m/Pa.s as PEG concentration increases from 0 to 6 wt% and it decreases to 2.2 $x10^{-11}$ m/Pa.s for 10 wt% PEG. However, pore density decreases upto 8 wt% and increases at 10 wt%. Since, the membrane becomes denser at 10 wt% compared to 8 wt%, the number of pores per square meter of membrane increases for 10 wt%. But, increase in pore density and decrease in pore size balance in such way that the permeability of 8 wt% and 10 wt% PEG 200 remains almost invariant. Variation of permeability with membrane composition confirms the observations presented in sections 3.2 and 3.3.

### 3.5 Molecular Weight Cut Off (MWCO) and Contact Angle

Variations of MWCO and contact angle for various membranes are shown in Fig. 4. Effects of molecular weight of PEG are presented in Fig. 4(a) and those of their concentration are shown in Fig. 4(b). The observations in this figure are in direct corroboration with the effect of PEG molecular weight as shown in SEM image (Figs. 2a). MWCO of the membranes increases from 38 to 106 kDa as molecular weight of PEG increases from 200 to

6000 Da. Since, hydrophilicity increases with molecular weight of PEG, contact angle decreases. The corresponding change is from $67^0$ to $47^0$.

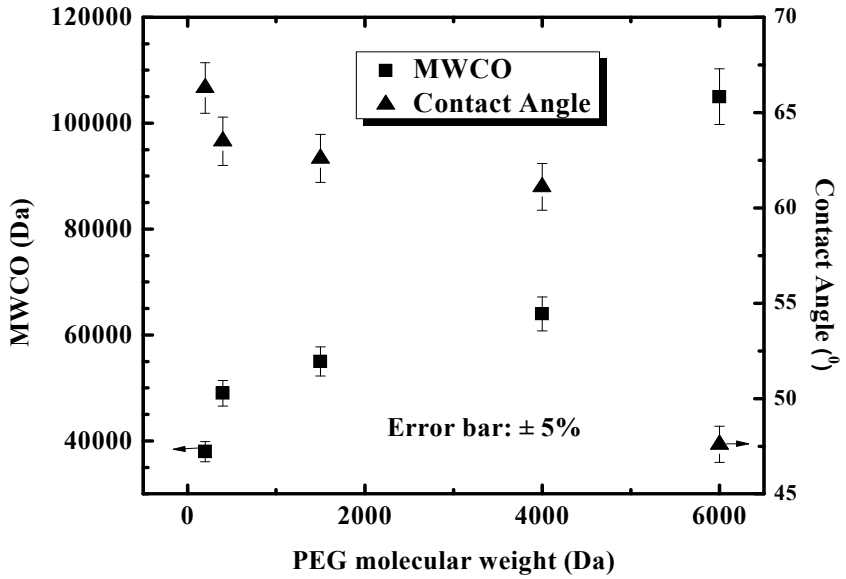


**Fig 4(a)**: MWCO and Contact Angle with variation of PEG Molecular weight

The effects of PEG concentration are evident from Fig. 4(b). As discussed earlier, the membrane becomes more porous upto 6 wt% of PEG, thereby, increasing MWCO from 38 to 56 kDa. Membranes become denser beyond this concentration and hence the MWCO decreases to 39 kDa. The trend of contact angle is in line with the variation of membrane permeability. As the permeability increases upto 6 wt% PEG, the membrane becomes more hydrophilic and its contact angle decreases from 72 to $55^0$. Beyond 6 wt%, the permeability decreases inducing more hydrophobicity on the membrane surface. Contact angle increases to $65^0$ when PEG concentration increases to 10 wt%.

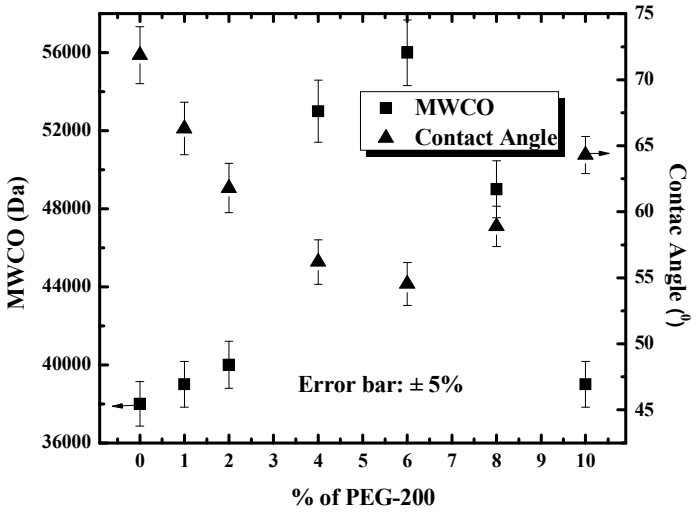


**Fig 4(b)**: MWCO and Contact Angle with variation of concentration of PEG-200.

### 3.6 Pore Size Distribution

As described earlier, cumulative pore volume ($cm^3/g$) distribution of the membranes are measured using BET surface area analyzer. Four typical pore size distributions corresponding to 0 wt%, 6 wt%, 10 wt% of PEG-200 and PEG 6000 1wt% are presented in Fig. 5.

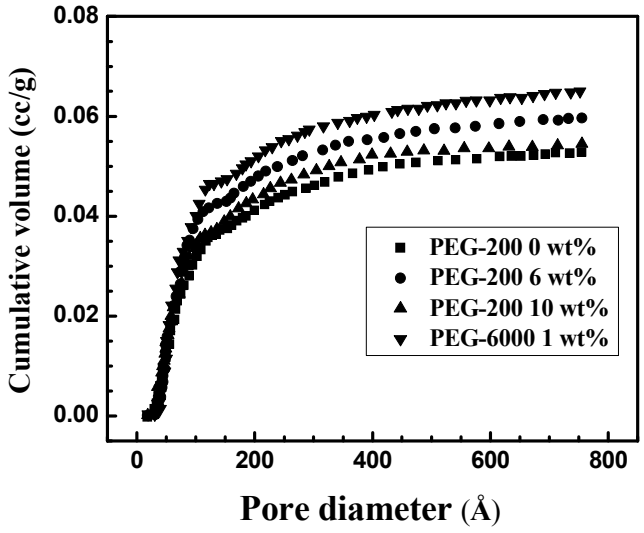


**Fig. 5**: Variation of Pore volume distribution with PEG-200 concentration and PEG molecular weight.

It is clear from Fig. 5, that cumulative pore volume for 6 wt% of PEG-200 is more than that of no PEG (0 wt%). This indicates that number of pores and permeability of membrane with 6 wt% PEG are more than that of no PEG. This measurement is in corroboration with kinetic hindrance, thermodynamic parameter in section 3.2, SEM images in (Fig. 2b) and permeability values (Fig. 3b) of these two membranes. On the other hand, 10 wt% of PEG 200, cumulative pore volume is less than that of 6 wt%. This clearly indicates that membrane with 10 wt% PEG is denser than 6 wt%. Again this observation confirms the trends shown in SEM images (Fig. 2b) and permeability values (Fig. 3b).

**Table 4:** Comparison of pore radius from Eq. (4) and BET analysis

| Synthesized membrane | Pore radius from MWCO correlation (Å) | Average pore radius from BET surface area analysis (Å) |
|---|---|---|
| **PEG-200 0 wt%** | 59±1.5 | 79±4 |
| **PEG-200 1 wt%** | 60±3 | - |
| **PEG-200 2 wt%** | 61±4 | - |
| **PEG-200 4 wt%** | 72±2.5 | - |
| **PEG-200 6 wt%** | 74±2.6 | 89±3 |
| **PEG-200 8 wt%** | 68±1.7 | - |
| **PEG-200 10 wt%** | 60±4 | 80±4 |
| **PEG-400 1 wt%** | 68±3.5 | - |
| **PEG-1500 1 wt%** | 73±2.3 | - |
| **PEG-4000 1 wt%** | 79±2.8 | - |
| **PEG-6000 1 wt%** | 105±1.8 | 92±3 |

As presented in Table 4, average pore size of membrane with 6 wt% PEG is 89 Å that is higher than 10 wt% PEG which is 80 Å. Membrane with no PEG has average pore size about 79 Å. This shows that average pore size of 10 wt% PEG 200 and that of no PEG is almost same. But membrane with no PEG has higher permeability (5.5 $x10^{-11}$ m/Pa.s) compared to 10 wt% PEG (2.2 $x10^{-11}$ m/Pa.s). This is due to the fact that pore density of membrane without PEG is much higher (1.7 $x10^{16}$ /$m^2$) compared to that of 10 wt% PEG membrane (6.4 $x10^{15}$ /$m^2$). Interestingly, the MWCO values of these two membrane are quite close, i.e., about 38 kDa. This trend is in accordance with cumulative pore size distribution of these two membrane measured by BET as shown in Fig. 5, and also the average pore size presented in Table 4. Thus, MWCO and permeability of the membrane are not one-to-one always. Cumulative pore volume for membrane with 1 wt% PEG 6000 is also shown in Fig 6. It shows that as observed in SEM images, this membrane is more porous and its average pore size is 105 Å that is in confirmation with permeability (26 $x10^{-11}$ m/Pa.s) and MWCO of this membrane (105 kDa).

### 3.7 Atomic force microscopy (AFM)

Three-dimensional AFM images of the typical four membranes corresponding to 0, 6 and 10 wt% of PEG-200 and PEG 6000 are presented in Fig. 6. It is observed from this figure (Figs. 6a and 6b) that more bumpy structure on top surface appears as the concentration of PEG increases. PEG is a well-known hydrophilic substance, accumulates more on the top surface during phase inversion. With increase in concentration on PEG, more PEG molecules compete for their place in upper layer of the membrane. Thus, average surface roughness increases from 70 to 133 nm as the concentration of PEG increases from 0 to 6 wt%. This trend also confirms the observation made by Sadeghi et al.,[57] that surface roughness increases for more porous membrane. As observed in Fig. 3(b), permeability of 6 wt% PEG membrane ($9 \times 10^{-11}$ m/Pa.s) is more than that without PEG ($5.5 \times 10^{-11}$ m/Pa.s). However, for 10 wt% PEG (Fig. 6c), the average roughness decreases to 94 nm. There are two opposing phenomena interplay in this case. First, more PEG molecules would like to come to the surface as its concentration is high that would enhance surface roughness. Second, at 10 wt% PEG, water influx to the membrane matrix is highly impeded (as discussed earlier) and a dense morphology sets in. Dense membranes have lower surface roughness.[58] The second effect becomes dominant as 10 wt% PEG concentration and the surface roughness becomes less (94 nm). For PEG 6000, bigger PEG molecules accumulate near the surface making it quite rough with average roughness of 188 nm.

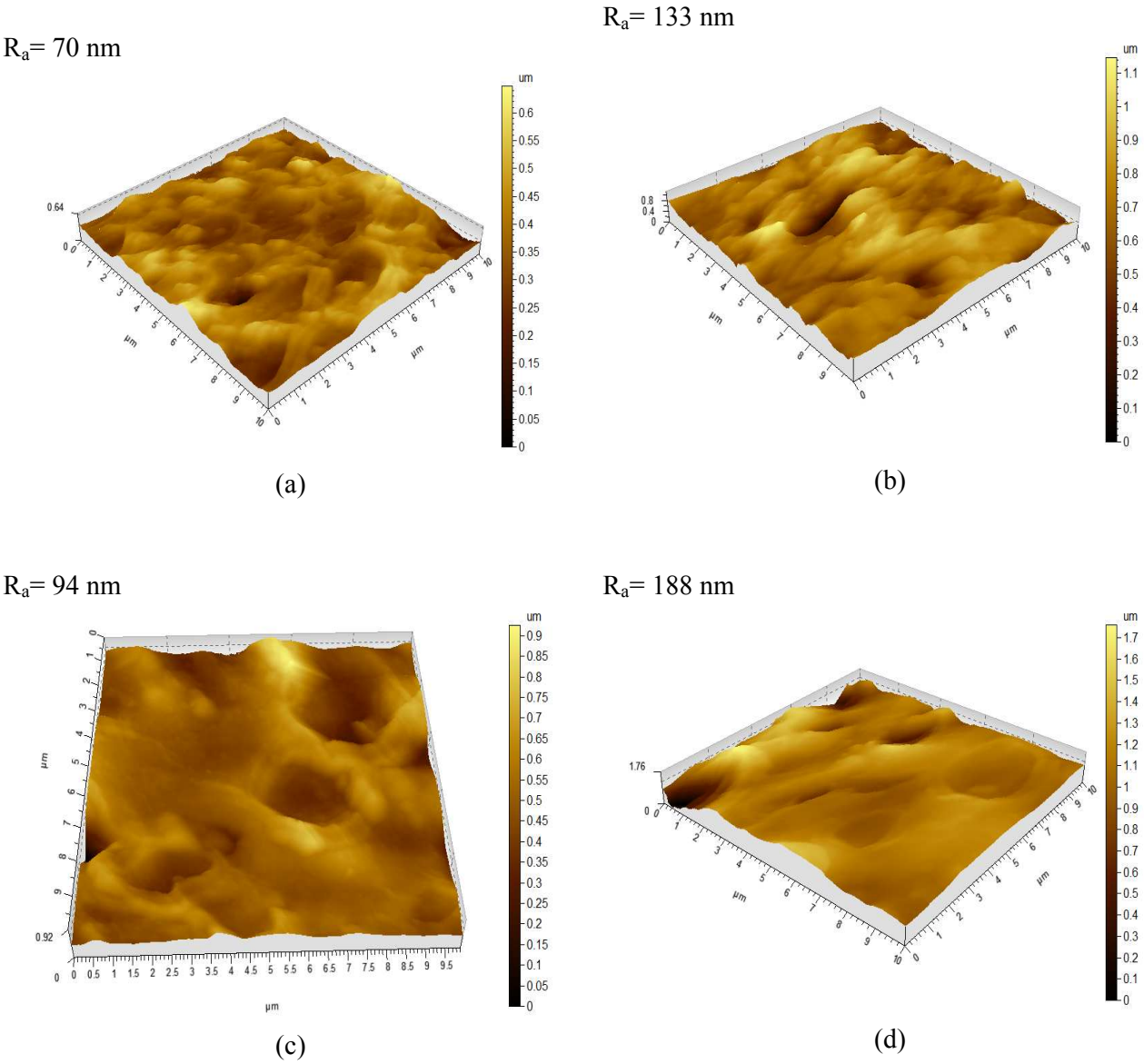


**Fig. 6**: Atomic force microscopy (AFM) images of membranes (a) PEG-200 0 wt%, (b) PEG-200 6 wt%, (c) PEG-200 10 wt%, (d) PEG-6000 1 wt%.

### 3.8 Tensile strength

Variation of breaking stress with PEG molecular weight and its concentration is presented in Fig. 7. Since the membrane becomes more porous with PEG molecular weight, breaking stress is also reduced. For example, breaking stress decreases from 18 to 16 MPa as the molecular weight of PEG increases from 200 to 6000 Da. Similarly, the membrane

500 becomes more porous upto 6 wt% of PEG, thereby, deteriorating the breaking stress upto that
501 concentration. Beyond, 6 wt%, membrane becomes dense, improving the breaking stress.

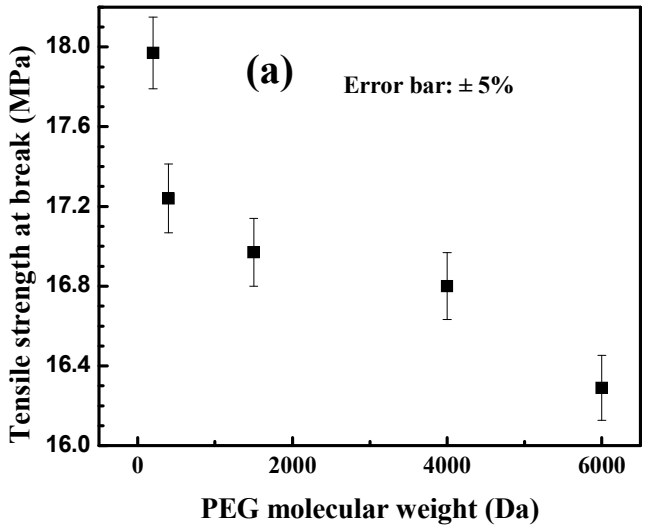


502

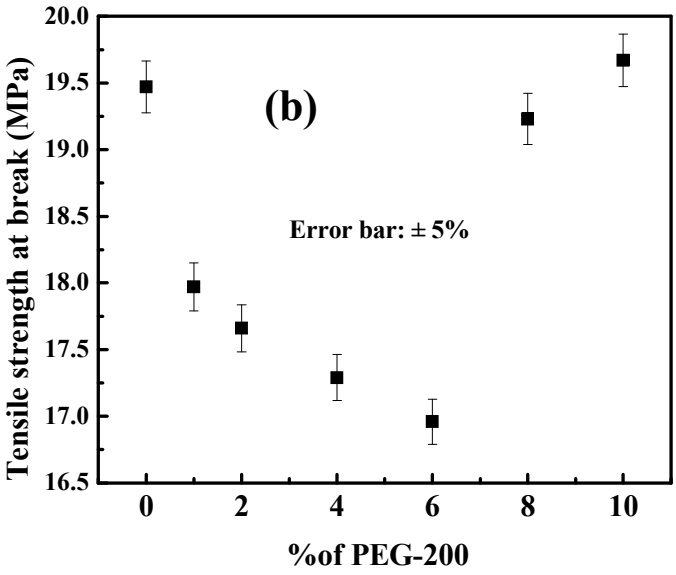


503

504 **Fig. 7**: Tensile strength with the variation of (a) PEG Molecular weight, (b) concentration of
505 PEG-200.

506

507

508

509

### 3.9 Differential scanning calorimetry:

DSC thermogram of the PAN-CAP blend membrane and those with different PEG additives are presented in Fig. 8. It is observed from this figure that PAN-CAP blend membrane and membranes with PEG show single glass transition temperature ($T_g$) indicating that the polymers are compatible. The possible interaction between nitrile group of PAN and hydroxyl group of CAP is schematically presented in Fig. 9. $T_g$ value is the highest 89 $^0$C for PAN-CAP blend membrane and it is the lowest for 1 wt% PEG 6000 (82 $^0$C). It is known that lowest $T_g$ of membrane shows porous structure[59, 60] and this observation is in corroboration with the observations made in earlier sections.

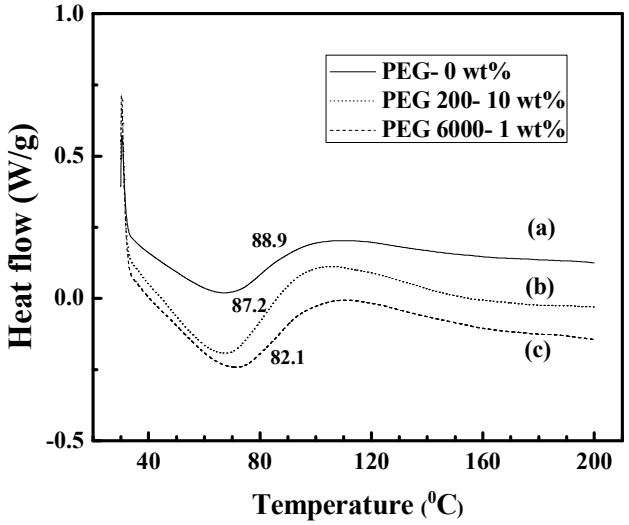


**Fig. 8**: Differential scanning calorimetry (DSC) curves for (a) PEG-200 0 wt%, (b) PEG-200 10 wt%, (c) PEG-6000 1 wt% membrane.

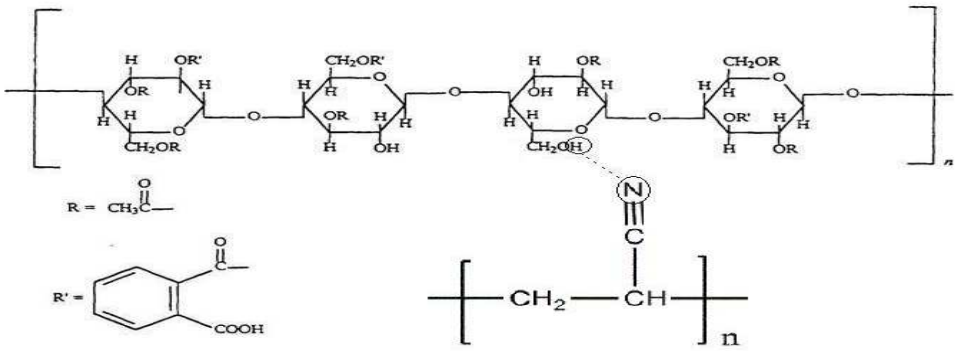


**Fig. 9**: Possible interaction of PAN with CAP.

524 **3.10 Permeate flux decline for BSA solution**

525 Profiles of permeate flux for BSA solution (0.5 kg/m$^3$) for various membranes are
526 shown in Fig. 10. It is observed from Fig. 10(a) that flux values at a particular time of
527 filtration is more for 200, 400, 4000 and 6000 Da PEG in that order. This is in corroboration
528 with the permeability values of these membranes. For a particular membrane, permeate flux
529 declines over the filtration period due to concentration polarization.[61] The flux decline trends
530 for different concentration of PEG are shown in Fig. 10(b). Again, the flux profiles are in the
531 same order of permeability values of these membranes. At a fixed time, the permeate flux
532 increases from 0 to 6 wt% PEG and it decreases for 8 and 10 wt%.

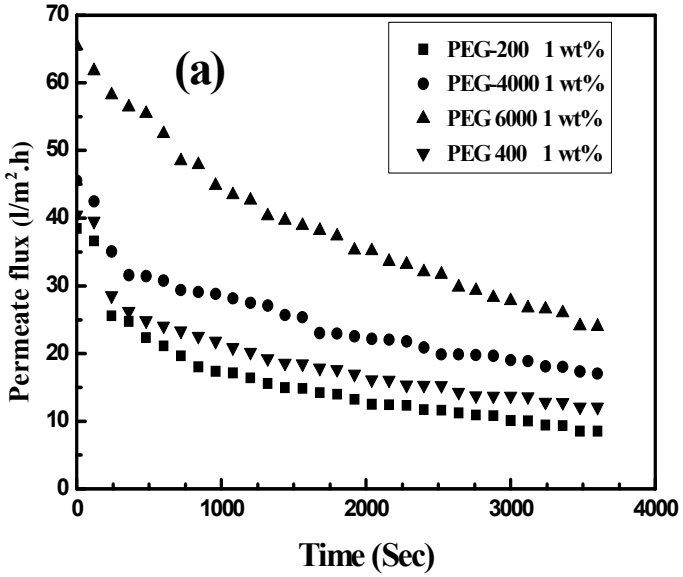


533

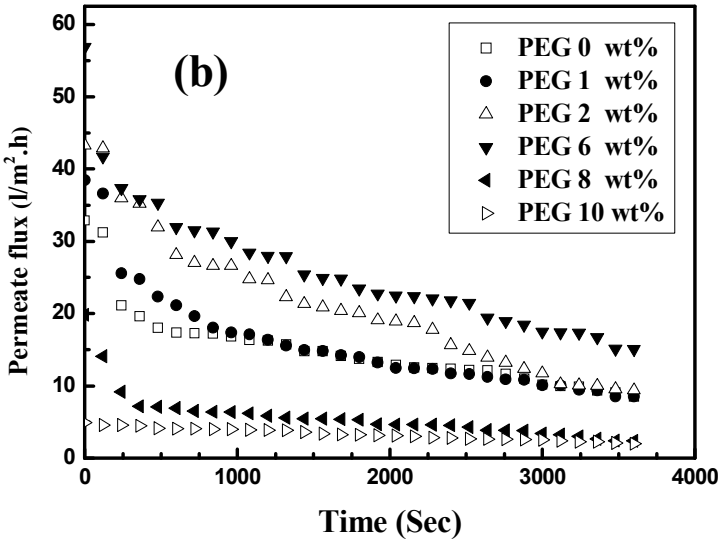


534

535 **Fig. 10**: Permeate flux variation of BSA solution with different (a) molecular weight of PEG,
536 (b) concentration of PEG-200.

537

538

539

540

541

542

### 3.11 Rejection and permeate flux of BSA solution

Rejection of BSA by various membranes and the permeate flux at the end of 1 hr are shown in Fig. 11.

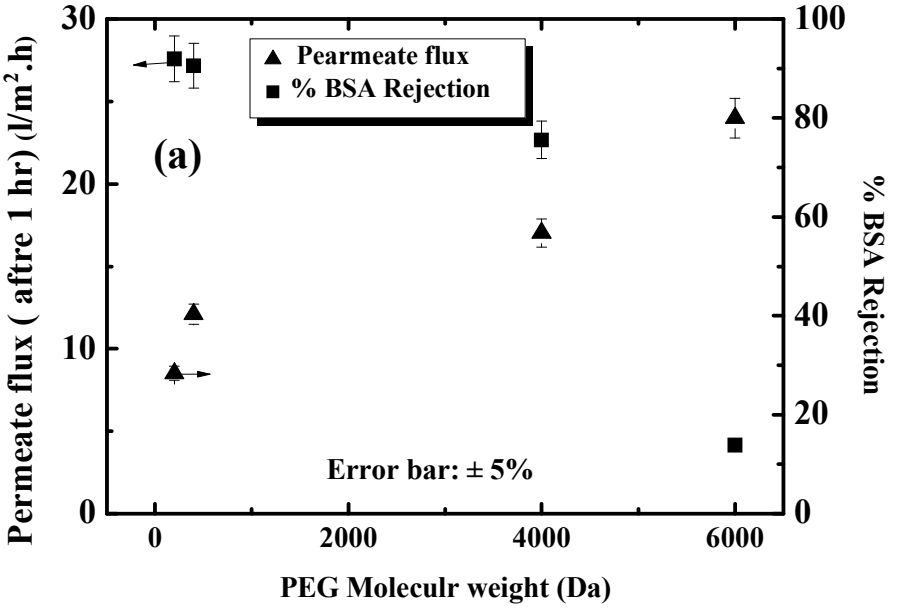


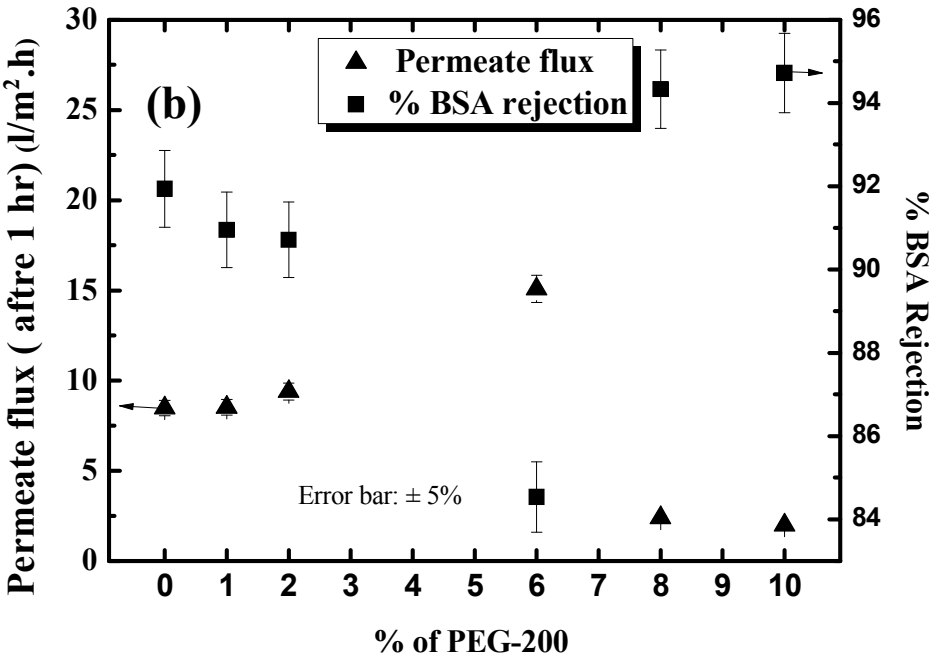


**Fig. 11**: Permeate flux after 1 hr and BSA rejection with variation of different (a) molecular weight of PEG, (b) concentration of PEG-200.

The flux values are in the expected trend as discussed earlier. BSA rejection can be explained according to variation of MWCO of these membranes. Since, the MWCO of the membranes increases with PEG molecular weight (Fig. 4a), rejection of BSA decreases in that order. Thus, BSA rejection decreases from 95% to 12% as the molecular weight of PEG increases from 200 to 6000 due to increase in pore size of the membrane (refer Fig. 10a). Similarly, variation of BSA rejection with PEG concentration is in direct corroboration with MWCO of these membranes. As the MWCO of membranes increases upto 6 wt% PEG, rejection of BSA decreases from 92 to 84%. Membrane MWCO decreases upto 10 wt% leading to corresponding increase in rejection to 95%. A brief comparison study of BSA rejection by various tailor made membranes is described in Table 5.

**Table 5:** Comparison of the BSA rejection

| Authors Name | Polymer | Additive (PEG) | Solvent | % BSA Rejection |
|---|---|---|---|---|
| Chakrabarty et al.[62] | PSF 12 wt% | 400 Da,6000 Da and 20000 Da 0 to 5 wt% | NMP and DMAc | 11 to 56.4 % |
| Ma et al.[63] | PSF 18 wt% | 400 Da, 800 Da 1500 Da, 4000 Da, 10000 Da, 20000 Da 0 to 10 wt% | DMAc | 40 to 90 % |
| Vijayalakshmi et al.[64] | CA/PC | 600 Da 0 to 10 wt% | NMP | 70 to 95 % |
| Amirilargani et al.[65] | PES/PAN | 400 Da, 600 Da, 1500 Da, 6000 Da | DMF | 74.8 to 93.8 % |
| Present Study | CAP/PAN | 200 Da, 400 Da, 1500 Da, 6000 Da 1 to 10 wt% | DMF | 14 to 94.72 % |

It is observed from this table that lower concentration of polysulfone (PSF) leads to low rejection (maximum 56%) of BSA.[62] However, higher concentration of PSF (18 wt%) and lower molecular weight of PEG lead to higher rejection of BSA upto 90%.[63] CA based membrane are reported BSA rejection from 70 to 95% corresponding to various concentration of PEG, as additive.[64] Amirilargani et al.,[65] reported BSA rejection in between 75 to 94% corresponding to various molecular weight of PEG in PES/PAN blend membrane. In the present case, PAN/CAP blend membrane exhibits a wide range of BSA rejection (14 to 95%) for various molecular weight of PEG (200 to 6000 Da) in the concentration range 1 to 10 wt%. Thus, the present membrane is comparable with the reported ones with respect to BSA rejection.

### 3.12 FRR and FDR

Antifouling capacities of various membranes are quantified in terms of FRR and FDR. Thus, highest FRR, lowest FDR and moderately high retention of BSA indicate the antifouling characteristics of the membranes. From Fig. 12(a), it is observed that membrane with PEG 200 shows FRR 60% and FDR 78%. Membrane with 6000 Da PEG shows maximum 80% FRR and about 65% FDR. On the other hand, PEG 200 results 91% rejection of BSA and PEG 6000 shows only 14% rejection. Thus, considering rejection of BSA as one factor, membrane with PEG 200 is desirable.

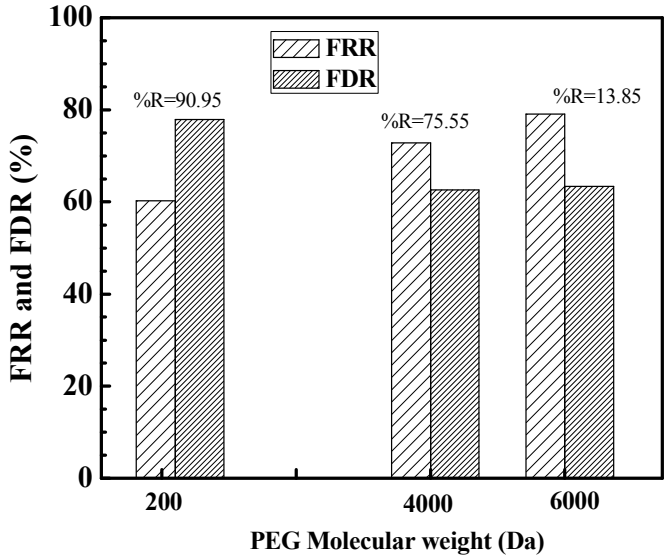


**Fig. 12(a)**: Flux recovery ratio (FRR) and Flux decline ratio (FDR) of membrane with variation of different molecular weight of PEG

Effects of PEG concentration on antifouling performance are shown in Fig. 12(b). It is observed that for all membranes, rejection of BSA is above 85%. For 8 and 10 wt% PEG, rejection is about 95%. But, FRR values are quite poor in both cases (about 50%). On the other hand, performance of 2 and 6 wt% PEG membranes is quite close. FRR values are 75 and 78%, respectively and corresponding FDR values are 77 and 75%. 2 wt% PEG rejects 91% BSA and 6 wt% rejects 84% PEG. Therefore, as per antifouling properties are concerned both of these membranes perform equally well.

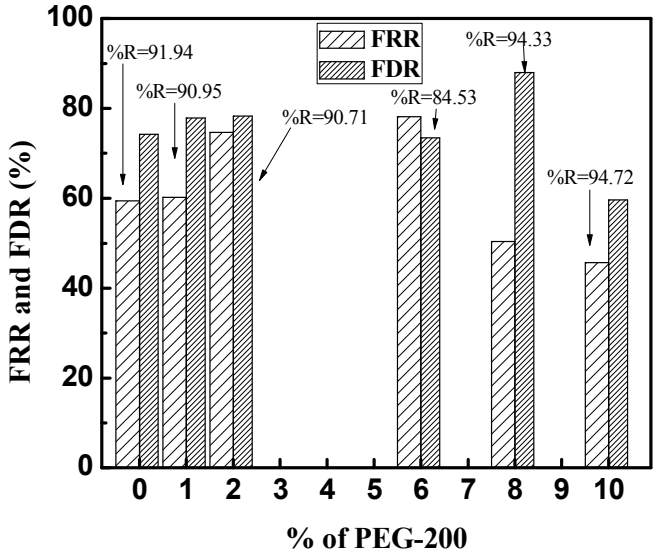


**Fig. 12(b)**: Flux recovery ratio (FRR) and Flux decline ratio (FDR) of membrane with variation of different concentration of PEG-200.

It is interesting to note the hydrophilic and antifouling properties of the developed membranes with similar types reported in literature. PAN based membrane was reported to have contact angle $60^0$ for 8 wt% of PEG 400 with MWCO 74 kDa[45] and for PSF based membrane it was $67^0$ for 10 wt% of PEG 400 with MWCO 55 kDa.[52] In the present work, 6 wt% PEG 200 in PAN-CAP blend reduces the contact angle further to $55^0$ with MWCO 56 kDa. Therefore, PEG added PAN-CAP blend results in more hydrophilic membrane with reduced MWCO compared to PAN-PEG membrane and equivalent MWCO with respect to PSF-PEG one. PEG added PAN-CAP blend membrane shows more antifouling characteristics compared to PAN-PEG membrane for 500 mg/l BSA solution. FDR value of PAN-PEG membrane is more than 82% and that of PAN-CAP-PEG membrane is less than 72% whereas, rejection of BSA in both membranes is comparable. Therefore, use of PEG additive in PAN-CAP blend results in more hydrophilic and antifouling membrane compared to PSF-PEG and PAN-PEG blend.

## 4.0 Conclusion

Effects of PEG as an additive on the characteristics and performance of PAN-CAP blend membrane have been investigated in detail. The following conclusion can be drawn from this study:

(i) Increase in molecular weight of PEG results into more porous membrane. Permeability of the membrane increases from 6 $x10^{-11}$ m/Pa.s to 26 $x10^{-11}$ m/Pa.s as the molecular weight of PEG increases 200 to 6000 Da. On the other hand pore density decreases with PEG molecular weight. Thus, increase in permeability is resulted from increase in pore size to the membrane not by increase in pore density.

(ii) Permeability of membrane increases upto 6 wt% PEG 200 (9 $x10^{-11}$ m/Pa.s) and it decreases to 2.5 $x10^{-11}$ m/Pa.s thereafter.

(iii) MWCO of the membrane increases from 38 K to 105 K at molecular weight of PEG increases from 200 to 6000 Da. Corresponding contact angle decreases from $66^0$ to $47^0$, making the membrane more hydrophilic.

(iv) MWCO becomes maximum 56 K at 6 wt% PEG 200 and it is reduced to 38 K at 10 wt%. Contact angle decreases to $54^0$ at 6 wt% PEG and increases to $65^0$ at 10 wt%.

(v) Both 2 wt% and 6 wt% PEG 200 showed equal antifouling properties. Theses membranes resulted to FRR values 75 and 78%, FDR values 77 and 75% and BSA rejection 91% and 84%, respectively.

## 5. Acknowledgements

This work is partially supported by a grant from the Board of Research in Nuclear Sciences, Department of Atomic Energy, Government of India, Mumbai, under the scheme no. 2012/21/03-BRNS, Dt. 25-07-2012. Any opinions, findings and conclusions expressed in this paper are those of the authors and do not necessarily reflect the views of BRNS.

## Nomenclature

| | |
|---|---|
| $A_0$ | Membrane surface area, $m^2$ |
| $C_P$ | Concentration of permeate, $kg/m^3$ |
| $C_F$ | Concentration of feed, $kg/m^3$ |
| $C_t$ | Concentration of solvent in coagulation bath at time t, $kg/m^3$ |
| $C_\infty$ | Concentration of solvent in coagulation bath at infinite time, $kg/m^3$ |
| $\hat{C}_{ns}$ | Volume fraction of pure nonsolvent |

| | | |
|---|---|---|
| 651 | $D_m$ | Diffusion coefficient of solvent, $m^2/s$ |
| 652 | *DSBC* | Degree shift in binodal curve, Eq. (A1) |
| 653 | *FRR* | Flux recovery ratio, Eq. (7) |
| 654 | *FDR* | Flux decline ratio, Eq. (8) |
| 655 | $J_w$ | Pure water flux, $m^3/m^2.s$ |
| 656 | $J_{w1}$ | Water flux of the membrane before experiment, $m^3/m^2.s$ |
| 657 | $J_{w2}$ | Water flux of the membrane after experiment, $m^3/m^2.s$ |
| 658 | $J_1$ | Initial flux of the membrane with BSA, $m^3/m^2.s$ |
| 659 | $J_s$ | Flux at the end of one hour, $m^3/m^2.s$ |
| 660 | *K* | Kinetic hindrance parameter, Eq. (A7) |
| 661 | *M* | Mass of the cast film, Kg |
| 662 | *MG* | Miscibility gap, Eq. (A1) |
| 663 | *L* | Membrane thickness, m |
| 664 | $n_c$ | Pore density, number of pore/$m^2$ |
| 665 | *Q* | Volumetric flow rate, $m^3/s$ |
| 666 | *R* | Rejection, % |
| 667 | $r_{avg}$ | Average pore size, m |
| 668 | *T* | Thermodynamic enhancement parameter, Eq. (A2) |
| 669 | $t_0$ | Time lag for sensing organics in the coagulation bath, s |
| 670 | *V* | Fixed volume of nonsolvent into which the solvent diffuses, $m^3$ |
| 671 | $V_1$ | Molar volume of the solvent, $m^3$/mol |
| 672 | | |
| 673 | **Greek Symbol** | |
| 674 | $\delta$ | Solubility parameters |
| 675 | $\Delta P$ | Transmembrane pressure drop, kPa |
| 676 | $\Delta T_0$ | Sampling time, s |
| 677 | $\gamma$ | Cast film compaction factors |
| 678 | $\chi$ | Interaction parameter between additive and the solvent, Eq. (A2) |
| 679 | $\mu$ | Viscosity of water, Pa.s |
| 680 | | |
| 681 | | |
| 682 | | |
| 683 | | |

**Reference:**


1 S.S. Madaeni, *Water Res.*, 1999, **33**, 301–308.

2 B. Nicolaisen, *Desalination*, 2002, **153**, 355-360.

3 J. Radjenovic, M. Petrovic, F. Venturac and D. Barcelo, *Water Res.*, 2008, **42**, 3601–3610.

4 Y. He, Z. Ji and S. Li, *Sep. Purif. Technol.*, 2007, **57**, 366–373.

5 M. Mulder, Kluwer Academic Publishers, Dordrecht, 1997.

6 M.J. Han and S.T. Nam, *J. Membr. Sci.*, 2002, **202**, 55–61.

7 B. Jung, J.K. Yoon, B. Kima and H.W. Rheeb, *J. Membr. Sci.*, 2004, **243**, 45–57.

8 Y. Liu, G.H. Koops and H. Strathmann, *J. Membr. Sci.*, 2003, **223**, 187–199.

9 W.Y. Chuang, T.H. Young, W.Y. Chiu and C.Y. Lin, *Polymer*, 2000, **41**, 5633–5641.

10 J.H. Kim and K.H. Lee, *J. Membr. Sci.*, 1998, **138**, 153–163.

11 M. Amirilargani, E. Saljoughi and T. Mohammadi, *Desalination*, 2009, **249**, 837–842.

12 M. Amirilargani, E. Saljoughi and T. Mohammadi, *J. Appl. Polym. Sci.*, 2010, **115**, 504–513.

13 E. Saljoughi and T. Mohammadi, *Desalination*, 2009, **249**, 850–854.

14 A. Rahimpour and S.S. Madaeni, *J. Membr. Sci.*, 2007, **305**, 299–312.

15 E. Saljoughi, M. Sadrzadeh and T. Mohammadi, *J. Membr. Sci.*, 2009, **326**, 627–634.

16 B. Jung, J.K. Yoon, B. Kima and H.W. Rheeb, *J. Membr. Sci.*, 2004, **243**, 45-57.

17 Y. Liu, Y. Su, Y. Li, X. Zhao and Z. Jiang, *RSC Adv.*, 2015, **DOI:** 10.1039/C4RA16290K

18 M.A. Phadke, S.S. Kulkarni, S.K. Karode and D.A. Musale, *J. Polym. Sci., Part B: Polym. Phys.*, 2005, **43**, 2074-2085.

19 S. Yang and Z. Liu, *J. Membr. Sci.*, 2003, **222**, 87-98.

20 L.E.S. Brink, S.J.G. Elbers, T. Robbertsen and P. Both, *J. Membr. Sci.*, 1993, **76**, 281-291.

21 A.V.R. Reddy, D.J. Mohan, A. Bhattacharya, V.J. Shah and P.K. Ghosh, *J. Membr. Sci.*, 2003, **214**, 211-221.

22 Y. Su, W. Cheng, C. Li and Z. Jiang, *J. Membr. Sci.*, 2009, **329**, 246-252.

23 X. Yang, B. Zhang, Z. Liu, B. Deng, M. Yu, L. Li, H. Jiang and J. Li, *J. Mater. Chem.*, 2011, **21**, 11908-11915

24 M. Ulbricht and A. Oechel, *Eur. Polym. J.*, 1996, **32**, 1045-1054.

25 J. Frahn, G. Malsch and F.H. Schwarz, *Macromol. Symp.*, 2001, **164**, 269-276.

26 T.D. Tran, S. Mori and M. Suzuki, *Thin Solid Films*, 2007, **515**, 4148-4152.

27 M. Ulbricht and G. Belfort, *J. Membr. Sci.*, 1996, **111**, 193-215.

28 M. Sivakumar, R. Malaisamy, C.J. Sajitha, D. Mohan, V. Mohan and R. Rangarajan, *J. Membr. Sci.*, 2000, **169**, 215-228.

29 M. Sivakumar, D. Mohan and R. Rangarajan, *Part 1, Polym. Int.*, 1998, **47**, 311-316.

30 M. Sivakumar, R. Malaisamy, C.J. Sajitha, D. Mohan, V. Mohan and R. Rangarajan, *Eur. Polym. J.*, 1999, **35**, 1647-1651.

31 M. Sivakumar, D. Mohan and R. Rangarajan, *J. Membr. Sci.*, 2006, **268**, 208–219.

32 E. Saljoughi, M. Amirilargani and T. Mohammadi, *Desalination*, 2010, **262**, 72–78.

33 G. Arthanareeswaran, S. Velu and L. Muruganandam, *J. Polym. Engg.*, 2011, **31,** 125-131.

34 L. Wu, J. Sun and Q. Wang, *J. Membr. Sci.*, 2006, **285**, 290-298.

35 S. Nie, M. Tang, C. Cheng, Z. Yin, L. Wang, S. Suna, and C. Zhao, *Biomater. Sci.*, 2014, **2,** 98-109.

36 L. Ma, H. Qin, C. Cheng, Y. Xia, C. He, C. Nie, L. Wanga and C. Zhao, *J. Mater. Chem. B*, 2014, **2**, 363-375.

37 H. Zhou, C. Cheng, H. Qin, L. Ma, C. He, S Nie, X. Zhang, Q. Fua and C. Zhao, *Polym. Chem.*, 2014, **5**, 3563-3575.

38 L. Wanga, B Su, C. Cheng, L. Ma, S. Li, S Nie and C. Zhao, *J. Mater. Chem. B*, 2015, **3**, 1391-1404.

39 Z. Yin, C. Cheng, H Qin, C. Nie, C. He and C Zhao, *J. Biomed. Mater. Res. Part B Appl. Biomater.*, 2015, **103**, 97–105.

40 X. Liu, J. Deng, L. Ma, C. Cheng, C. Nie, C. He and C. Zhao, *Langmuir*, 2014, **30**, 14905–14915.

41 A. V. R. Reddy and H. R. Patel, *Desalination*, 2008, **221**, 318–323.

42 M. C. Yang and T. Y. Liu, *J. Membr. Sci.*, 2003, **226**, 119–130.

43 Y. Xiuli, C. Hongbin, W. Xiu and Y. Yongxin, *J. Membr. Sci.*, 1998, **146**, 179-184.

44 A. Roy and S. De, *J. Food Eng.*, 2014, **126**, 7-16.

45 S. R. Panda and S. De, *Polym. Eng. Sci.*, 2014, **54**, 2375-2391.

46 N. Schamagl and H. Buschatz, *Desalination*, 2001, **139**, 191-198.

47 B. Jung, J. K. Yoon, B. Kim and H.W. Rhee, *J. Membr. Sci.*, 2004, **243**, 45-57.

48 J. W. Lim, J. M. Lee, S. M. Yun, B. J. Park and Y. S. Lee, *J. Ind. Eng. Chem.*, 2009, **15**, 876–882.

49 E. Shekarian, E. Saljoughi and A. Naderi, *J. Polym. Res.*, 2013, **20**, 1‑9.

50 J. Wang, Z. Yue, J.S. Ince and J. Economy, *J. Membr. Sci.*, 2006, **286**, 333-341.

51 X. Chen, Y. Su, F. Shen and Y. Wan, *J. Membr. Sci.*, 2011, **384**, 44-51.

52 S.R. Panda and S. De, *J. Polym. Res.*, 2013, **20**, 179-195.

53 M. Sadrzadeh and S. Bhattacharjee, *J. Membr. Sci.*, 2014, **441**, 31–44.

54 J.F. Li, Z.L. Xu, H. Yang, L.Y. Yu and M. Liu, *Appl. Surf. Sci.*, 2009, **255**, 4725-4732.

55 S. Singh, K.C. Khulbe, T. Matsuura and P. Ramamurthy, *J. Membr. Sci.*, 1998, **142**, 111-127.

56 I.C. Kim and K.H. Lee, *J. Membr. Sci.*, 2004, **230**, 183-188.

57 I. Sadeghi, A. Aroujalian, A. Raisi, B. Dabir and M. Fathizadeh, *J. Membr. Sci.*, 2013, **430**, 24-36.

58 R.R. Olmos, E.R. Hernandez, L.Z.F. Lopez, S.W. Lin and H.E. Gomez, *J. Chil. Chem. Soc.*, 2008, **53**, 1705-1708.

59 M. Ali, M. Zafar, T. Jamil and M. T. Z. Butt, *Desalination*, 2011, **270**, 98-104.

60 S. R. Panda and S. De, *RSC Adv.*, 2015, **5**, 23599- 23612.

61 M.C. Porter, Crest Publishing House, New Delhi, India, 2005.

62 B. Chakrabarty, A.K. Ghoshal and M.K. Purkait, *J. Membr. Sci.*, 2008, **309**, 209-221.

63 Y. Ma, F. Shi, J. Ma, M. Wu, J. Zhang and C. Gao, Desalination, 2011, **272**, 51-58.

64 A. Vijayalakshmi, D.L. Arockiasamy, A. Nagendran and D. Mohan, *Sep. Purif. Technol.*, 2008, **62**, 32-38.

65 M. Amirilargania, A. Sabetghadama and T. Mohammadia, *Polym. Adv. Technol.*, 2012, **23**, 398-407.

66 J.H. Kim, B.R. Min, H.C. Park, J. Won and Y.S. Kang, *J. Appl. Polym. Sci.*, 2001, **81**, 3481–3488.

67 L. Shuguang, J. Chengzhang and Z. Yuanqi, Desalination, 1987, **62**, 79–88.

68 A.F.M. Barton, 2nd Ed., CRC Press, Boca Raton, FL, 1991.

69 D.W. Van Krevelen and K.T. Nijenhuis, 4th Ed., Elsevier, 2009.

70 J.F. Li, Z.L. Xu, H. Yang, C.P. Feng and J.H. Shi, *J. Appl. Polym. Sci.*, 2007, **107**, 4100–4108.

71 C. Özdemir and A. Güner, *Eur. Polym. J.*, 2007, **43**, 3068–3093.

72 M. Maniruzzaman, J.S. Boateng, M. Bonnefille, A. Aranyos, J.C. Mitchell and D. Douroumis, *Eur. J. Pharm. Biopharm.*, 2012, **80**, 433–442.

73 A.V. Patsis and E.H. Henriques, *J. Polym. Sci. Part B: Polym. Phys.*, 1990, **28**, 2681–2689.

74 A. C. Sun, W. Kosar, Y. Zhang and X. Feng, *Desalination*, 2013, **309**, 156–164.

## Appendix A

### A.1 Estimation of thermodynamic parameter

The distance between polymer-solvent axis and the part of binodal curve parallel to this axis is MG. Degree of shift in binodal curve (DSBC) indicates the thermodynamic change of the casting solution due to addition of additive. DSBC is estimated as follows,[66]

$$DSBC = \frac{MG_{w/o\ additive} - MG_{w/\ additive}}{MG_{w/o\ additive}} \times 100\% \quad \text{(A1)}$$

Thus, overall thermodynamic enhancement parameter, $T$ of polymer due to additive is quantified as[67]

$$T = DSBC \times \chi_{solvent/additive} \quad \text{(A2)}$$

where, $\chi_{solvent/additive}$ is the interaction parameter between additive and the solvent. For no additive, T is zero and large value of T indicates enhanced thermodynamic instability leading to quick demixing and formation of porous membrane. $\chi_{solvent/additive}$ in above equation is Flory-Huggins solvent polymer interaction parameter and is calculated as[67]

$$\chi_{solvent/additive} = \frac{V_1}{RT}(\delta_{solvent} - \delta_{additive})^2 \quad \text{(A3)}$$

where, $V_1$, $R$ and $\delta$ are molar volume of the solvent, ideal gas constant and solubility parameters, respectively. Molar volume of solvent DMF was $V_1$= 77.09 $cm^3mol^{-1}$.[68] Group contribution method is used to calculate the solubility parameter of additives of different molecular weight.[69-72] Hansen solubility parameters of additives and DMF are presented in Table A1. Literature data was used for calculation of solubility parameters of DMF.[68]

**Table A1:** Hansen solubility parameters of additives and DMF

| Material | $n$ ($MW_p$/ $MW_m$) | $\rho$ (g $cm^{-3}$) | $V$ ($cm^3mol^{-1}$) | $\delta_d$ $(MPa)^{1/2}$ | $\delta_p$ $(MPa)^{1/2}$ | $\delta_h$ $(MPa)^{1/2}$ | $\delta_t$ $(MPa)^{1/2}$ |
|---|---|---|---|---|---|---|---|
| PEG 0.2 kDa | 4 | 1.128 | 177 | 15.65 | 5.33 | 13.45 | 21.31 |
| PEG 1.5 kDa | 34 | 1.10 | 1364 | 16.10 | 1.74 | 9.45 | 18.75 |
| PEG 6 kDa | 136 | 1.07 | 5607 | 15.56 | 0.8367 | 8.74 | 17.44 |
| DMF[55] | ----- | ----- | ----- | 17.4 | 13.7 | 11.30 | 24.86 |

### A.1.1 Calculation of Hansen Solubility Parameter:

Interactions between dispersion forces ($\delta_d$), polar interactions ($\delta_p$) and hydrogen bonding ($\delta_h$) of the structural groups are considered to estimate Hansen solubility parameter ($\delta_t$):

$$\delta_t^2 = \delta_d^2 + \delta_p^2 + \delta_h^2 \quad \text{(A4)}$$

where $\delta_d$, $\delta_h$ and $\delta_p$ are calculated using the group contribution method.[69-72]

### A.2 Kinetic hindrance effect due to additives

This effect can be quantified by diffusion of solvent in the coagulation bath and the concentration profile of solvent is represented by the following equation,[53, 73, 74]

$$\frac{C_t}{C_\infty} = \frac{\sqrt{2}AC_mD_m}{V\sqrt{\gamma \hat{C}_{ns} D_{ns}}}(t^{0.5} - t_0^{0.5}) \quad \text{(A5)}$$

where, $\gamma$, $D_m$, $C$, $A$, $\hat{C}_{ns}$, $C_t$, $C_\infty$, $V$ and $t_0$ are cast film compaction factors, diffusion coefficient of solvent, volume fraction, area of the cast film, volume fraction of pure nonsolvent ($\hat{C}_{ns}$=1), concentration of solvent in coagulation bath at time t, concentration of solvent in coagulation bath at infinite time, fixed volume of nonsolvent into which the solvent diffuses and time lag for sensing organics in the coagulation bath. Therefore, a plot between $C_t/C_\infty$ versus $t^{0.5}$ results in a straight line with slope ($m$)

$$m = \frac{\sqrt{2}AC_mD_m}{V\sqrt{\gamma \hat{C}_{ns} D_{ns}}} = \frac{\sqrt{2}AC_m}{V\sqrt{\gamma \hat{C}_{ns}}}\frac{D_m}{\sqrt{D_{ns}}} = \beta\frac{D_m}{\sqrt{D_{ns}}} \quad \text{(A6)}$$

From above equation, knowing the values of $V$=1000 cm$^3$, $A$=232 cm$^2$, $\hat{C}_{ns}$=1 and $\gamma$=1, the ratio $D_m/\sqrt{D_{ns}}$ is estimated. The dimensionless kinetic hindrance parameter is expressed,[42]

$$K = \frac{D_m}{\sqrt{D_{ns}}}\frac{M}{A\mu t_0^{0.5}} \quad \text{(A7)}$$

where, $M$, $A$ and $\mu$ are mass, surface area and viscosity of the cast film, respectively.

The kinetic data on the polymer precipitation was measured by the solvent leaching rate.[53, 73, 74]The polymer solution was cast on the non-woven fabric (attached to a glass plate) at room temperature and then it was immediately put into a deionized water bath. Samples were taken from the gelation bath using a micro syringe. The solvent concentration in

coagulation bath was measured with time in terms of refractive index using a digital refractometer (M/s, Cole-Parmer, Kolkata, India).

### A.2.1 Estimation of kinetics parameter

The solvent concentration ($C_t/C_\infty$) in the coagulation bath for different polymer composition is shown in Fig. A1. It is observed from this figure that rate of solvent-nonsolvent demixing increases for 10 wt% PEG 200, 6 wt% PEG 200, PEG 1500 (1 wt%) and PEG 6000 Da (1 wt%), in that order. Additive increases the viscosity of casting solution, promoting kinetic hindrance.

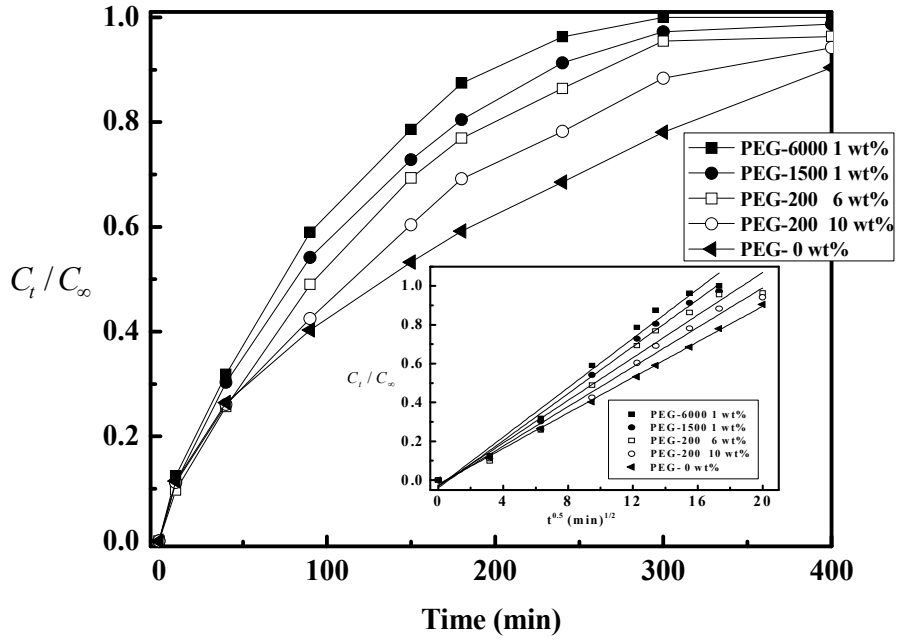


**Fig. A1.** Kinetic properties of various casting solutions